ACS APPLIED MATERIALS & INTERFACES

Research Article

www.acsami.org

Two-Dimensional Porous Micro/Nano Metal Oxides Templated by Graphene Oxide

Hailiang Cao, Xufeng Zhou,* Chao Zheng, and Zhaoping Liu*

Advanced Li-ion Battery Engineering Lab, Ningbo Institute of Materials Technology and Engineering (NIMTE), Chinese Academy of Sciences, Zhejiang, 315201, China

Supporting Information

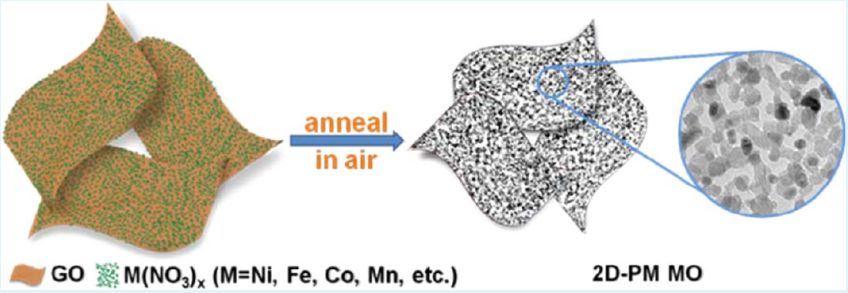

ABSTRACT: Novel two-dimensional (2D) porous metal oxides with micro-/nanoarchitecture have been successfully fabricated using graphene oxide (GO) as a typical sacrificial template. GO as a 2D template ensures that the growth and fusion of metal oxides nanoparticles is restricted in the 2D plane. A series of metal oxides (NiO, Fe_2O_3, Co_3O_4, Mn_2O_3, and $NiFe_2O_4$) with similar nanostructure were investigated using this simple method. Some of these special nanostructured materials, such as NiO, when being used as anode for lithium-ion batteries, can exhibit high specific capacity, good rate performance, and cycling stability. Importantly, this strategy of creating a 2D porous micro/nano architecture can be easily extended to controllably synthesize other binary/polynary metal oxides nanostructures for lithium-ion batteries or other applications.

KEYWORDS: *graphene, metal oxides, two dimensional, nanostructure, lithium-ion battery*

1. INTRODUCTION

Metal oxides (MOs) belong to an important class of functional materials for various applications.[1−4] In particular, MOs and their assemblies have been widely utilized in all kinds of fundamental research and technological applications due to their unique properties and potential for desired nanostructures.[5−7] Over the past decades, nanostructured MOs have undergone a booming development. It is well-known that the size, morphology, and structure of nanomaterials significantly influence their physical and chemical properties and their applications.[8−10] Micro-/nanostructures, where the particles are typically of micro-/submicrometer dimensions but internally consist of nanobuilding units, are of great significance to advance the practical applications.[11] The unique micro-/nanostructures with hierarchical architecture can endow MOs with exceptional merits from both nanosized building blocks and micro-/submicrometer assemblies. Many efforts have been devoted to the controlled synthesis of various micro/nano MOs with different nanostructures, which have demonstrated great potential of micro-/nanostructures in various application fields.[12−14] However, a tremendous amount of works are needed to explore novel micro-/nanomaterials to further improve their performance for wider and more challenging applications, such as energy storage, catalysis, and chemical sensing.

Graphene, a single layer of sp^2-bonded carbon atoms, is an intriguing two-dimensional material and has attracted much attention mainly due to its outstanding physical and chemical properties.[15−17] Graphene oxide (GO), which can be obtained easily by oxidizing graphite powders, is often adopted as the precursor to prepare graphene and also has the same two-dimensional structure.[18,19] More importantly, there are plenty of oxygen-containing functional groups on the basal plane and edge of GO, which are active sites for chemical reaction with various substances. In numerous previous studies, GO was often used as a substrate to load various active materials to fabricate different functional materials because of its high surface area and relatively high conductivity after being reduced. Relatively little attention has been paid to investigate the framework substitution of GO.[20]

In this work, we have successfully realized the preparation of novel two-dimensional porous micro/nano (2D-PM) MOs, in which MO nanoparticles connect each other in the two-dimensional plane to form a sheetlike microstructure with plenty of nanosized pores, by using GO as a two-dimensional sacrificial template. The unique architecture offers the MOs high specific capacity and excellent rate capability and cycling

Received: March 6, 2015
Accepted: May 21, 2015
Published: May 21, 2015

DOI: 10.1021/acsami.5b02014
ACS Appl. Mater. Interfaces 2015, 7, 11984−11990

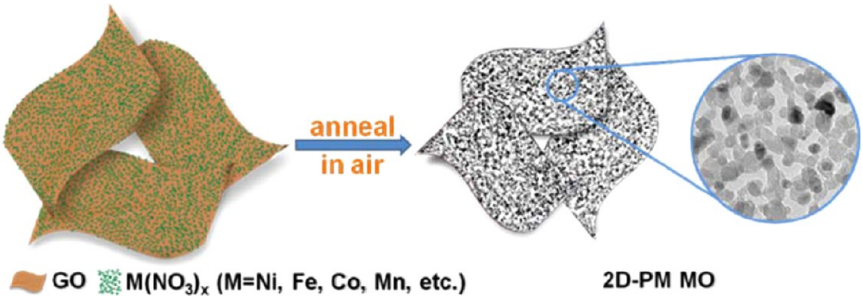

Figure 1. Schematic illustration for the synthesis of the 2D-PM MO.

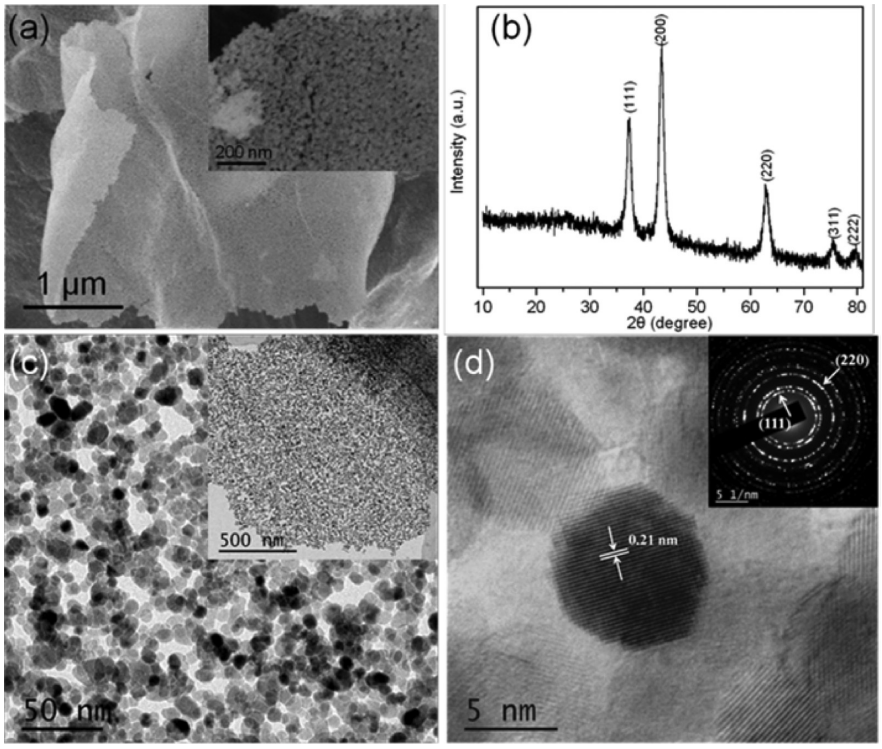

Figure 2. Low-magnification and high-magnification (inset) SEM image (a) and XRD pattern (b) of the 2D-PM NiO. The low-magnification (inset) and high-magnification TEM image (c) and high-resolution TEM image (d) of 2D-PM NiO; the inset of (d) shows the SAED pattern.

stability for use as anode materials in lithium-ion batteries (LIBs).

2. EXPERIMENTAL SECTION

2.1. Preparation of 2D-PM MOs. GO was synthesized using a modified Hummer's method.[21] To prepare 2D-PM NiO structure, nickel nitrate hexahydrate of the desired ratio was dissolved in 20 mL of deionized water and then 20 mL of GO solution (4 mg mL^{-1}) was added under vigorous stirring. The mass ratio of GO/Ni was 10/1. After sonication, the final solution was frozen in a fridge (−18 °C), transferred into freeze-drying equipment, and evaporated in vacuum at the temperature below 0 °C for 2 days. The dry mixture power was heated from room temperature to 600 °C at a rate of 10 °C min^{-1} in a tube furnace and held at this temperature for 3 h under air to obtain the brown powder NiO. The mass ratio of GO/Ni, holding time, and annealing temperature were adjusted in our experiments.

To prepare other 2D-PM MOs, iron(III) nitrate nonahydrate, cobalt(II) nitrate, and manganous nitrate instead of nickel nitrate were used with the same procedure, respectively. For preparation of binary transition-metal oxide $NiFe_2O_4$, iron(III) nitrate and nickel nitrate need to be mixed first with desired ratio.

2.2. Sample Characterization. Power X-ray diffraction (XRD) patterns were recorded on an AXS D8 Advance diffractometer with Cu Kα radiation. Scanning electron microscopy (SEM) and transmission electron microscopy (TEM) images were acquired using a field emission SEM (S-4800, Hitachi) and an FEI Tecnai G2 F20 TEM, respectively.

2.3. Electrochemical Measurement. The electrochemical properties of the 2D-PM NiO electrodes were measured with CR2032 coin cells. First, the paste was prepared by mixing active material and Super P (SP) with poly(vinylidene fluoride) (PVDF) in *N*-methyl-2-pyrrolidinone solution. The weight ratio of active material:SP:PVDF was 80:10:10, and then the paste was coated on Cu foil and dried at 100 °C for 24 h in vacuum. After that, the resultant film was punched into 13 mm diameter discs as anode. Last, the coin cells were assembled in an argon-filled glovebox using polypropylene film as separator. $LiPF_6$ (1 M) dissolved in a mixture of ethylene carbonate and dimethyl carbonate (1:1, by volume) was employed as electrolyte. The galvanostatic charge/discharge tests were carried out within a voltage range of 0.01−3 V on a cell testing system (LAND CT2001A, China). The cyclic voltammogram (CV) was performed using the Solartron 1400 cell test system with a scan rate of 0.1 mV s^{-1}. All the tests were conducted at constant temperature (25 °C).

DOI: 10.1021/acsami.5b02014
ACS Appl. Mater. Interfaces 2015, 7, 11984−11990

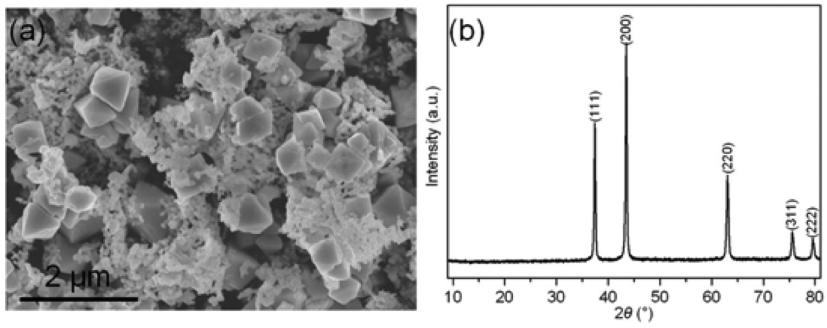

Figure 3. SEM image (a) and XRD pattern (b) of NiO prepared by annealing nickel nitrate at 600 °C in air.

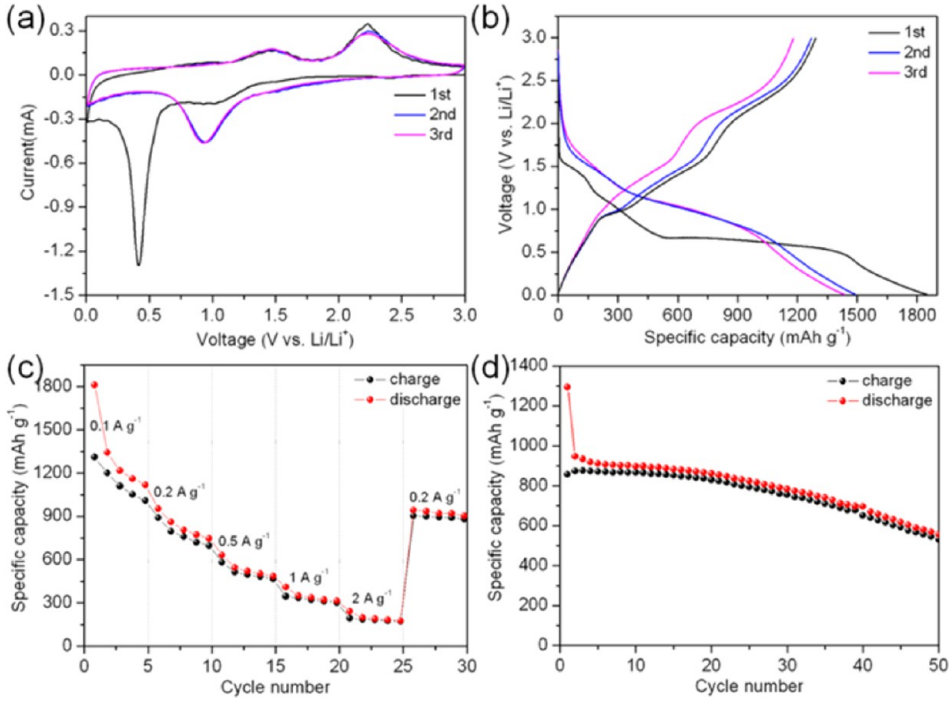

Figure 4. Electrochemical performance of the 2D-PM NiO anode in LIBs. CV profile (a) and charge/discharge curves (b) of NiO for the first three cycles at the current density of 50 mA g^{-1}. (c) Rate performance of NiO between 0.01 and 3.0 V with increasing current density. (d) The cycling performance of the 2D-PM NiO at a current density of 0.2 A g^{-1}.

3. RESULTS AND DISCUSSION

As illustrated in Figure 1, the first step to prepare 2D-PM MO is homogeneous mixing of GO and metal nitrate in solution, followed by freeze-drying to obtain a solid mixture. The solid powder was then subjected to thermal treatment in air. During this process metal nitrate first decomposed to form MO nanoparticles, and then at high-temperature MO nanoparticles grow up gradually and connect each other to form porous micro-/nanoarchitecture. GO template was removed completely by combustion simultaneously.

In our experiment, NiO was initially selected as the typical research system. The elemental mapping analysis of the GO and $Ni(NO)_2$ solid mixture (see Figure S1 in the Supporting Information) shows that the whole basal plane of GO sheets contains a large amount of Ni with a uniform distribution density besides numerous C and O, evident of homogeneous scattering of $Ni(NO)_2$ on the GO surface. After heat treatment, the obtained NiO shows typical 2D sheetlike morphology as displayed in Figure 2a and Figure S2, which is quite similar to the structure of GO, implying that GO plays an important role in directing the formation of 2D microstructure of NiO. It is notable that the NiO sheet is so thin that other sheets under the surface are also faintly visible. SEM image with a higher magnification (inset of Figure 2a) indicates that the sheet is not a dense one, but has plenty of nanosized pores. The XRD pattern of the NiO is shown in Figure 2b. The diffraction peaks observed at 2θ angles of 37.25°, 43.27°, 62.88°, 75.41°, and 79.41° can be indexed to the planes (111), (200), (220), (311), and (222) of cubic NiO (JCPDS No. 47-1049), respectively.[22,23] The broad widths of diffraction peaks indicate the small crystal size of NiO. The mean particle size is calculated to be ca. 8.5 nm using the Scherrer equation. TEM observation also reveals the two-dimensional porous micro-/nanostructure of NiO, as shown in Figure 2c. The low-magnification TEM image (inset in Figure 2c) confirms the 2D structure of NiO product with the lateral size of 2−3 μm, consistent with SEM result. In addition, Figure 2c demonstrates a highly porous structure formed by a network of NiO nanoparticles with the average size of ∼10 nm which is in agreement with the XRD result. The high-resolution TEM image of NiO in Figure 2d shows lattice fringes with interplanar spacing of 0.21 nm

DOI: 10.1021/acsami.5b02014
ACS Appl. Mater. Interfaces 2015, 7, 11984−11990

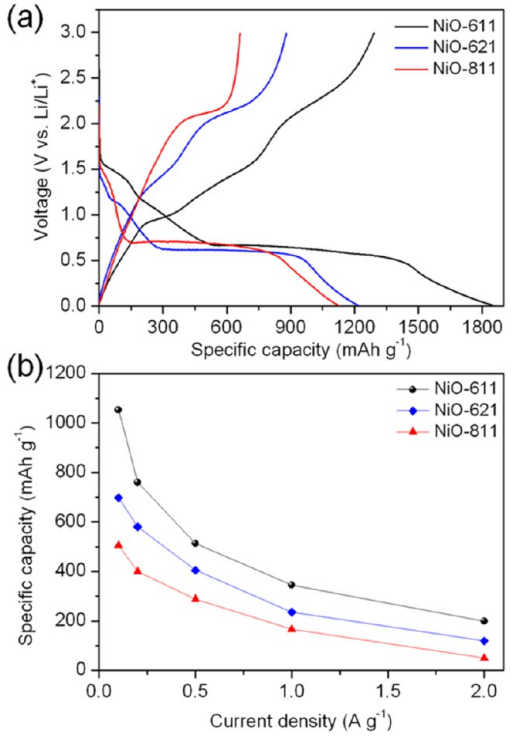

Figure 5. Charge/discharge curves (a) at 50 mA g^{-1} and rate performance (b) of NiO with different morphologies.

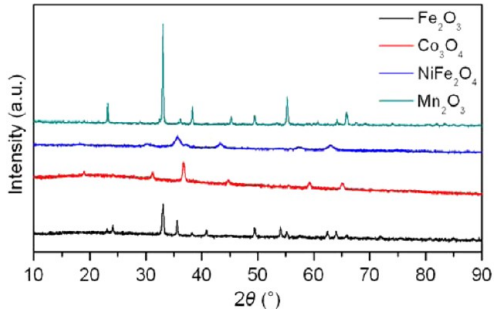

Figure 6. XRD patterns of the other metal oxides prepared with the same strategy.

corresponding to the (200) lattice plane. The selected area electron diffraction (SAED) pattern as an inset image in Figure 2d is in good agreement with the XRD pattern and demonstrates a polycrystalline structure of NiO. Therefore, in the present work we have successfully synthesized the 2D-PM NiO architecture, in which NiO nanoparticles with uniform size connect each other to form a micro/submicrometer scale sheet in the two-dimensional plane. More importantly, this kind of 2D-PM NiO has plenty of pores with even distribution, which is very helpful for ion diffusion and buffering the volume change during the charge/discharge process. Given these, the 2D-PM MOs may exhibit good electrochemical performance, which will be demonstrated later by testing 2D-PM NiO electrode.

To demonstrate the important role of the GO, nickel nitrate without mixing with GO was annealed merely in air for comparison. As shown in Figure 3a, no 2D sheetlike structure is observed. Instead, a mixture of submicrometer NiO particles with octahedron morphology and nonuniform NiO nanoparticles are obtained. The narrow diffraction peaks of the sample (Figure 3b) also indicate large crystal size, consistent with the SEM result. Furthermore, a series of experiments with varied reaction conditions were carried out to investigate the formation mechanism of the 2D-PM NiO. As shown in Figure S3, the mass ratio of GO/Ni was found to be critical to the structure of the 2D-PM NiO. The GO/Ni ratio of 10/1 is believed to be optimal to obtain uniform micro-/nanoarchitecture. Raising the Ni content to the GO/Ni ratio of 5/1 results in large Ni nanoparticles with less uniform size distribution, while less Ni content (GO/Ni of 15/1 and 20/1) gives rise to severe agglomeration of Ni nanoparticles. In addition, by lengthening the heating time from 1 to 3 h, the size of the NiO nanopaticles increases gradually from ~6 to ~10 nm (see Figure S4 in the Supporting Information). However, the size of the nanoparticles remains almost identical when further prolonging the heating time from 3 to 12 h. Moreover, the heating temperature is also a crucial factor to the final structure of the material. It can be observed that the morphologies of the obtained samples heated at different temperatures differ sharply (see Figure S5). The two-dimensional porous structure of NiO remains well at 500 and 600 °C. But the micro-/nanostructure is destroyed when the temperature is increased to 700 and 800 °C since adjacent NiO nanoparticles fuse and grow rapidly to large particles at such high temperatures. Therefore, on the basis of the above experimental results, there is no doubt in reaching the conclusion that GO plays a crucial role in preparation of MOs with two-dimensional porous micro-/nanoarchitecture. First, the abundant oxygen-containing groups of GO make uniform distribution of metal nitrate on the surface of GO, which is an essential step. During the decomposition of metal nitrate and formation of MO nanoparticles at high temperatures, GO can provide a two-dimensional template, ensuring that the growth and fusion of MO nanoparticles is restricted in the two-dimensional plane. Certainly, appropriate mass ratio of GO/Ni and annealing temperature are required to obtain even distribution and uniform size of the MO nanoparticles, as well as to control the fusion of adjacent nanoparticles to form homogeneous porous structure.

The lithium-storage properties of as-prepared 2D-PM NiO were investigated. Figure 4a shows the first three consecutive CVs over a potential range from 0.01 to 3.0 V at a scan rate of 0.1 mV s^{-1}. It is obvious that there are significant differences between the first scan and the subsequent scans. In the first cycle, a major reduction peak locating at around 0.4 V is observed, which corresponds to the initial reduction of Ni^{2+} to Ni^0 and the formation of a partially reversible solid electrolyte interface (SEI) layer.[24,25] This peak becomes broader and weaker, and shifts to about 1.0 V in the second and third cycles. The two oxidation peaks locating at 1.47 and 2.24 V can be ascribed to the formation of NiO and the decomposition of SEI, respectively.[26,27] The CV curves become identical after two cycles, indicating the reversible electrochemical process since the second cycle. The charge/discharge studies were also performed galvanostatically for porous NiO. Figure 4b shows the typical initial three charge/discharge curves at a current density of 50 mA g^{-1} within a voltage window of 0.01−3.0 V. In the first discharge process, the constant plateau between 0.66 and 0.35 V indicates the conversion reaction of NiO to Ni and the electrolyte decomposition, which is in good agreement with the CV analysis. With the benefits of the two-dimensional porous micro-/nanostructure, the first discharge and charge

DOI: 10.1021/acsami.5b02014
ACS Appl. Mater. Interfaces 2015, 7, 11984−11990

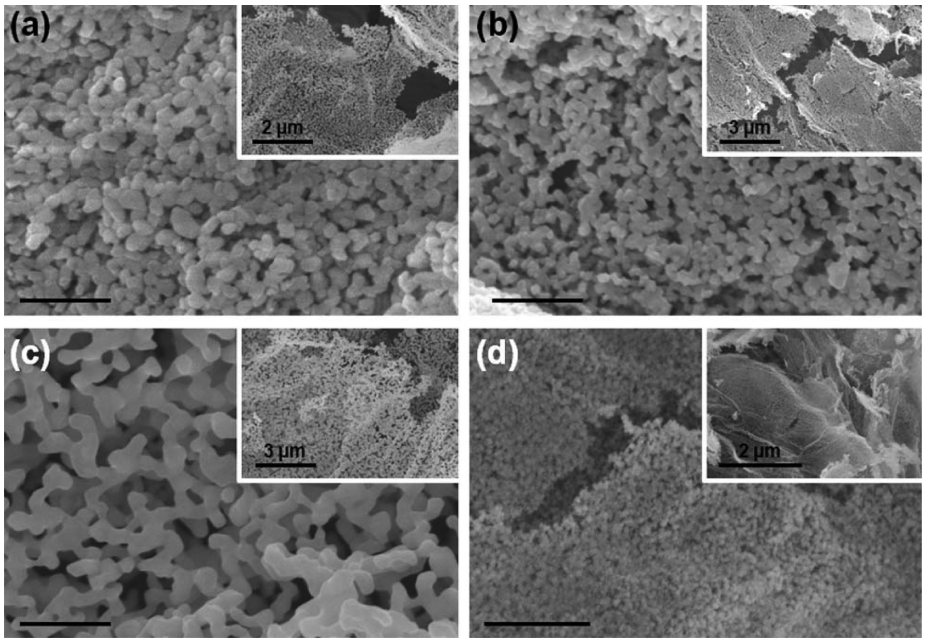

Figure 7. High-magnification and low-magnification (inset) SEM images of the other transition-metal oxides. (a) Fe_2O_3, (b) Co_3O_4, (c) Mn_3O_4, and (d) $NiFe_2O_4$. The scale bar is 500 nm.

specific capacity is as high as 1850 and 1340 mA h g^{-1}, respectively.

To further evaluate the rate performance of the 2D-PM NiO, charge/discharge cycling tests were performed under various current densities of up to 2 A g^{-1} (2.8 C, 1C = 718 mA h g^{-1}) as summarized in Figure 4c. The initial discharge and charge capacity at a low current density of 0.1 A g^{-1} are as high as 1810 and 1311 mA h g^{-1}, respectively. It can be found that the capacities decrease as the cycling current rates increase. Importantly, the capacity of NiO still maintains about 200 mA h g^{-1} even at a high current density of 2 A g^{-1}. When the current was brought down to 0.2 A g^{-1} after 25 cycles, a stable reversible capacity of 905 mA h g^{-1} could be recovered. The results indicate that the as-prepared 2D-PM NiO can tolerate high current charge/discharge cycling. The capacity versus cycle number at a current density of 0.2 A g^{-1} is shown in Figure 4d. It is notable that the specific capacity is relatively stable before the 20th cycles and no conspicuous capacity loss was observed. Although the capacity gradually fades afterward, the discharge and charge capacities of the NiO electrode still remain as high as 568 and 544 mA h g^{-1} in the 50th cycle, exhibiting excellent capacity retention capability.

In addition, three typical samples were chosen to investigate the effects of morphology on the electrochemical performances. The first sample is 2D-PM NiO prepared with the optimal condition, i.e., calcinated at 600 °C with the GO/Ni ratio of 10/1. The second was calcinated at 600 °C with the ratio of 20/1, and the third was calcinated at 800 °C with the ratio of 10/1. Three samples are denoted as NiO-611, NiO-621, and NiO-811, respectively, for convenience. The morphology and nanostructure of the three samples are notably different (Figure S3b for NiO-611, Figure S3d for NiO-621, and Figure S5d for NiO-811). The size of NiO increases from ~10 to ~200 nm through altering the synthesis condition. In addition, the three samples also exhibit significantly different electrochemical performances as depicted in Figure 5. At the current density of 50 mA g^{-1}, the first discharge and charge capacities are 1117.9 and 663 mAh g^{-1} for the NiO-811 sample, whereas the corresponding capacities for NiO-621 are 1216.4 and 879.2 mA h g^{-1}, respectively. Both samples show much lower capacities than those of NiO-611, demonstrating that the smaller size of NiO is favorable to deliver higher capacities. The result is consistent with the previous study.[28] Moreover, the NiO-611 sample shows superior rate performance. At all current density, the capacity of NiO-611 is always higher than that of NiO-621 and NiO-811. With increasing current density from 0.1 to 2 A g^{-1}, the capacity of NiO-811 decreases from 505 to 50 mA h g^{-1}, corresponding to a capacity retention of 10%, and the capacity of NiO-621 decreases from 698 to 119 mA h g^{-1} (17% capacity retention). However, the capacity of NiO-611 decreases from 1052 to 200 mA h g^{-1}, corresponding to improved capacity retention of 19%. From the above results, it can be concluded that rational design of the nanostructure of MOs by tuning the reaction conditions is necessary for seeking high electrochemical performance.

According to the results above, the electrochemical performance of the 2D-PM NiO is better compared to the reported performance of NiO with nanostructures such as nanotuble,[29] net structure,[30] microsphere,[31] and nanopowder.[32] The enhancement should be credited to the porous micro-/nanoarchitecture with two-dimensional features. As identified by SEM and TEM analysis, the two-dimensional NiO sheets consist of numerous small nanoparticles and plenty of pores. During the charge/discharge process, Li^+ is able to diffuse easily and react with single NiO nanoparticle through the pores. Furthermore, the abundant pores between the nanoparticles can provide structural flexibility for volume change.

Besides NiO, some other MOs with similar structure were also successfully prepared via the same procedure. The XRD patterns of the obtained samples (Figure 6) can be indexed to Fe_2O_3 (JCPDS No. 33-0664),[33] cubic spinel Co_3O_4 (JCPDS No. 43-1003),[34] and cubic Mn_2O_3 (JCPDS No. 41-1442),[35] respectively. It is worth noting that the binary transition-metal oxide spinel $NiFe_2O_4$ (JCPDS No. 10-0325)[36] can also be

DOI: 10.1021/acsami.5b02014
ACS Appl. Mater. Interfaces 2015, 7, 11984−11990

obtained. Figure 7 illustrates the typical morphologies of these samples. As expected, from the low-magnification SEM images (inset in each image), their morphologies are similar to the 2D-PM NiO, all maintaining the sheetlike structure of GO. Nevertheless, from the high-magnification SEM images, there are still some differences between these materials. The nanoparticles of Fe_2O_3 and Co_3O_4 are very similar and the average size of the two is 120 and 70 nm, respectively. The nanoparticles of the Mn_2O_3 are relatively large and fuse with each other to form coral-like structure. The size of the $NiFe_2O_4$ nanoparticles (~15 nm) is the smallest. The size of MOs particles may be related to the different activity of MOs at high temperature. The above results indicate that this strategy is also suitable for preparation of other MOs including binary MOs.

4. CONCLUSIONS

When GO was adopted as a structural templating agent, novel two-dimensional porous metal oxides with micro-/nano-architecture have been successfully prepared for the first time. GO was chosen as the typical two-dimensional template due to its unique structure and abundant oxygen functional groups. The novel nanostructure of as-prepared 2D-PM NiO, when applied as a LIBs anode material, exhibits a very high specific capacity and improved rate performance as well as cyclic stability. Meanwhile, a series of metal oxides (Fe_2O_3, Co_3O_4, Mn_2O_3, and $NiFe_2O_4$) with the similar nanostructure were investigated using the same method. Thus, this strategy of creating a 2D porous micro-/nanoarchitecture can be easily extended to synthesize other binary/polynary metal oxides nanostructures for LIBs or other applications.

■ ASSOCIATED CONTENT

Supporting Information

Experimental details, element mapping analysis of a mixture of GO and nickel nitrate, and SEM images of 2D-PM NiO prepared by different conditions. The Supporting Information is available free of charge on the ACS Publications website at DOI: 10.1021/acsami.5b02014.

■ AUTHOR INFORMATION

Corresponding Authors

*E-mail: liuzp@nimte.ac.cn. Fax: +86-574-8668-5096. Tel.: +86-574-8668-5096.

*E-mail: zhouxf@nimte.ac.cn. Fax: +86-574-8668-5096. Tel.: +86-574-8668-5096.

Notes

The authors declare no competing financial interest.

■ ACKNOWLEDGMENTS

This work was financially supported by the National Natural Science Foundation of China (Grant No. 21201173 and 21371176), Ningbo Science and Technology Innovation Team (Grant No. 2012B82001), and the Zhejiang Province Preferential Postdoctoral Fund Project (Grant No. Bsh 1302054).

■ REFERENCES

(1) Zarur, A. J.; Ying, J. Y. Reverse Microemulsion Synthesis of Nanostructured Complex Oxides for Catalytic Combustion. *Nature* **2000**, *403*, 65−67.

(2) Sattler, J. H. B.; Ruiz-Martines, J.; Stantillan-Jimen-ez, E.; Weckhuysen, B. M. Catalytic Dehydrogenation of Light Alkanes on Metals and Metal Oxides. *Chem. Rev.* **2014**, *114*, 10613−10653.

(3) Reddy, M. V.; Subba Rao, G. V.; Chowdari, B. V. R. Metal Oxides and Oxysalts as Anode Materials for Li Ion Batteries. *Chem. Rev.* **2013**, *113*, 5364−5457.

(4) Vohs, J. M. Site Requirements for the Adsorption and Reaction of Oxygenates on Metal Oxide Surfaces. *Chem. Rev.* **2013**, *113*, 4136−4163.

(5) Sun, S.; Zeng, H. Size-Controlled Synthesis of Magnetite Nanoparticles. *J. Am. Chem. Soc.* **2002**, *124*, 8204−8205.

(6) Patzke, G. R.; Zhou, Y.; Kontic, R.; Conrad, F. Oxide Nanomaterials: Synthesis Developments, Mechanistic Studies, and Technological Innovations. *Angew. Chem., Int. Ed.* **2010**, *49*, 2−36.

(7) Lao, J. Y.; Wen, J. G.; Ren, Z. F. Hierarchical ZnO Nanostructures. *Nano Lett.* **2002**, *2*, 1287−1291.

(8) Li, Y.; Shen, W. Morphology-Dependent Nanocatalysts: Rod-shaped Oxides. *Chem. Soc. Rev.* **2014**, *43*, 1543−1574.

(9) Jing, L.; Zhou, W.; Tian, G.; Fu, H. Surface Tuning for Oxide-Based Nanomaterials as Efficient Photocatalysts. *Chem. Soc. Rev.* **2013**, *42*, 9509−9549.

(10) Zhang, L.; Niu, W.; Xu, G. Synthesis and Applications of Noble Metal Nanocrystals with High-Energy Facets. *Nano Today* **2012**, *7*, 586−605.

(11) Yuan, C.; Wu, H. B.; Xie, Y.; Lou, X. W. Mixed Transition-Metal Oxides: Design, Synthesis, and Energy-Related Applications. *Angew. Chem., Int. Ed.* **2013**, *52*, 2−19.

(12) Lee, J. H. Gas Sensors using Hierarchical and Hollow Oxide Nanostructures: Overview. *Sens. Actuators, B* **2009**, *140*, 319−336.

(13) Kuang, Q.; Wang, X.; Jiang, Z.; Xie, Z.; Zheng, L. High-Energy-Surface Engineered Metal Oxide Micro- and Nanocrystallites and Their Applications. *Acc. Chem. Res.* **2014**, *47*, 308−318.

(14) Lai, X.; Halpert, J. E.; Wang, D. Recent Advances in Micro-/nano-Structured Hollow Spheres for Energy Applications: From Simple to Complex Systems. *Energy Environ. Sci.* **2012**, *5*, 5604−5618.

(15) Meyer, J. C.; Geim, A. K.; Katsnelson, M. I.; Novoselov, K. S.; Booth, T. J.; Rothh, S. The Structure of Suspended Graphene Sheets. *Nature* **2007**, *446*, 60−63.

(16) Geim, A. K.; Novoselov, K. S. The Rise of Graphene. *Nat. Mater.* **2007**, *6*, 183−191.

(17) Geim, A. K. Graphene: Status and Prospects. *Science* **2009**, *324*, 1530−1534.

(18) Zhu, Y.; Murali, S.; Cai, W.; Li, X.; Suk, J. W.; Potts, J. R.; Ruoff, R. S. Graphene and Graphene Oxide: Synthesis, Properties, and Applications. *Adv. Mater.* **2010**, *22*, 3906−3924.

(19) Chen, D.; Feng, H.; Li, J. Graphene Oxide: Preparation, Functionalization, and Electrochemical Applications. *Chem. Rev.* **2012**, *112*, 6027−6053.

(20) Chen, S.; Zhu, J.; Wang, X. From Graphene to Metal Oxide Nanolamellas: A Phenomenon of Morphology Transmission. *ACS Nano* **2010**, *4*, 6212−6218.

(21) Zhou, X.; Liu, Z. A Scalable, Solution-Phase Processing Route to Graphene Oxide and Graphene Ultralarge Sheets. *Chem. Commun.* **2010**, *46*, 2611−2613.

(22) Li, Q.; Chen, Y.; Yang, T.; Lei, D.; Zhang, G.; Mei, L.; Chen, L.; Li, Q.; Wang, T. Preparation of 3D Flower-like NiO Hierarchical Architectures and Their Electrochemical Properties in Lithium-Ion Batteries. *Electrochim. Acta* **2013**, *90*, 80−89.

(23) Kim, G.; Park, S.; Nam, I.; Park, J.; Yi, J. Synthesis of Porous NiO Materials with Preferentially Oriented Crystalline Structures with Enhanced Stability as Lithium Ion Battery Anodes. *J. Power Sources* **2013**, *237*, 172−177.

(24) Ni, S.; Li, T.; Yang, X. Fabrication of NiO Nanoflakes and Its Application in Lithium Ion Battery. *Mater. Chem. Phys.* **2012**, *132*, 1108−1111.

(25) Xie, D.; Yuan, W.; Dong, Z.; Su, Q.; Zhang, J.; Du, G. Facile Synthesis of Porous NiO Hollow Microspheres and Its Electrochemical Lithium-Storage Performance. *Electrochim. Acta* **2013**, *92*, 87−92.

(26) Debart, A.; Dupont, L.; Poizot, P.; Leriche, J. B.; Tarascon, J. M. A Transmission Electron Microscopy Study of Reactivity Mechanism

DOI: 10.1021/acsami.5b02014
ACS Appl. Mater. Interfaces 2015, 7, 11984−11990

of Tailor-made CuO Particles toward Lithium. *J. Electrochem. Soc.* **2001**, *148*, A1266−A1274.
(27) Grugeon, S.; Laruelle, S.; Herrera-Urbina, R.; Dupont, L.; Poizot, P.; Tarascon, J. M. Particles Size Effects on the Electrochemical Performance of Copper Oxides toward Lithium Batteries and Energy Conversion. *J. Electrochem. Soc.* **2001**, *148*, A285−A292.
(28) Cheng, M. Y.; Ye, Y. S.; Chiu, T. M.; Pan, C. J.; Hwang, B. J. Size Effect of Nickel Oxide for Lithium Ion Battery Anode. *J. Power Sources* **2014**, *253*, 27−34.
(29) Needham, S. A.; Wang, G. X.; Liu, H. K. Synthesis of NiO Nanotubes for Use as Negative Electrodes in Lithium Ion Batteries. *J. Power Sources* **2006**, *159*, 254−257.
(30) Huang, X. H.; Tu, J. P.; Zhang, C. Q.; Xinag, J. Y. Net-Structured NiO−C Nanocomposite as Li-Intercalation Electrode Material. *Electrochem. Commun.* **2007**, *9*, 1180−1184.
(31) Liu, L.; Li, Y.; Yuan, S.; Ge, M.; Ren, M.; Sun, C.; Zhou, Z. Nanosheet-Based NiO Microspheres: Controlled Solvothermal Synthesis and Lithium Storage Performances. *J. Phys. Chem. C* **2010**, *114*, 251−255.
(32) Huang, X. H.; Tu, J. P.; Zhang, B.; Zhang, C. Q.; Li, Y.; Yuan, Y. F.; Wu, H. M. Electrochemical Properties of NiO−Ni Nanocomposite as Anode Material for Lithium Ion Batteries. *J. Power Sources* **2006**, *161*, 541−544.
(33) Zhu, X.; Song, X.; Ma, X.; Ning, G. Enhanced Electrode Performance of Fe_2O_3 Nanoparticle-Decorated Nanomesh Graphene as Anodes for Lithium Ion Batteries. *ACS Appl. Mater. Interfaces* **2014**, *6*, 7189−7197.
(34) Rakhi, R. B.; Chen, W.; Cha, D.; Alshareef, H. N. Substrate Dependent Self-Organization of Mesoporous Cobalt Oxide Nanowires with Remarkable Pseudocapacitance. *Nano Lett.* **2012**, *12*, 2559−2567.
(35) Qiao, Y.; Yu, Y.; Guan, Y.; Chen, C. Synthesis and Electrochemical Properties of Porous Double-Shelled Mn_2O_3 Hollow Microspheres as a Superior Anode Material for Lithium Ion Batteries. *Electrochim. Acta* **2014**, *132*, 323−331.
(36) Yu, Z.; Chen, L.; Yu, S. Growth of $NiFe_2O_4$ Nanoparticles on Carbon Cloth for High Performance Flexible Supercapacitors. *J. Mater. Chem. A* **2014**, *2*, 10889−10894.

DOI: 10.1021/acsami.5b02014
ACS Appl. Mater. Interfaces 2015, 7, 11984−11990